Orange reflection from a three-dimensional photonic crystal in the scales of the weevil *Pachyrrhynchus congestus pavonius* (Curculionidae)

Victoria Welch,[1,2] Virginie Lousse,[1,3] Olivier Deparis,[1] Andrew Parker,[4] and Jean Pol Vigneron[1,*]
[1]*Laboratoire de Physique du Solide, Facultés Universitaires Notre-Dame de la Paix, 61 rue de Bruxelles, B-5000 Namur Belgium*
[2]*Department of Zoology, University of Oxford, South Park Road, Oxford, OX1 3PS, United Kingdom*
[3]*Ginzton Laboratory, Stanford University, Stanford, California 94305, USA*
[4]*Department of Zoology, The Natural History Museum, Cromwell Road, London, SW7 5BD, United Kingdom*
(Received 16 February 2007; published 30 April 2007)

The three-dimensional structure that causes the coloration of the tropical weevil *Pachyrrhynchus congestus pavonius* was studied, using a combination of electron microscopy, optical spectroscopy, and numerical modeling. The orange scales that cover the colored rings on the animal's body were opened, to display the structure responsible for the coloration. This structure is a three-dimensional photonic polycrystal, each grain of which showing a face-centered cubic symmetry. The measured lattice parameter and the observed filling fraction of this structure explain the dominant reflected wavelength in the reddish orange. The long-range disorder introduced by the grain boundaries explains the paradoxical observation that the reflectance, although generated by a photonic crystal, is insensitive to changes in the viewing angle.

DOI: 10.1103/PhysRevE.75.041919 PACS number(s): 42.66.−p, 42.70.Qs, 42.81.Qb

I. INTRODUCTION

Many living organisms have evolved transparent submicrometer structures that produce colors from light interference. Such structures have been identified in birds like the green peacock (*Pavo muticus*) [1] or the black-billed magpie (*Pica pica*) [2], both of which have two-dimensional photonic crystals in the cortex barbules of their feathers. Marine animals such as the sea mouse (*Aphrodita* spp.) [3] or the comb jellyfish (*Beroë cucumis*) [4] also show patterns of refractive index that produce a strong iridescence. The widest range of coloring structures has, however, been identified in insects, where butterflies and beetles from tropical regions provide innumerable examples of spectrally selective surfaces. A wide variety of structural reflectors have been observed in butterflies, which can be classified as multilayer structures [5–7], diffraction gratings [8,9], three-dimensional crystal lattices [10,11], and disordered aggregates of beads [12]. In beetles, the coloration can be produced in flat exocuticles or in identifiable scales. With the former, we often find layers of essentially isotropic materials—as in the metallic woodboring beetles [13]—or of anisotropic materials (see many Cetonidae), giving rise to a Bouligand, circularly polarizing structure [14]. With scales, the visual effect can be even more complex, as in the case of the blue beetle *Hoplia coerulea* [15] or the tropical weevils [16], which we will consider in the present work.

Weevils are a group of beetles that are feared and famed in equal measure for the devastation some species can inflict on agricultural production, horticulture, and human food stores, such as grain barns. There are thought to be in the region of 40 000 species of weevil and both larvae and adults feed—variously—on the leaves, roots, or fruits of specific plants, with a huge array of plants targeted among the different weevil species. There is, consequently, a large literature on this aspect of their biology.

The genus *Pachyrrhynchus* (also known as *Pachyrhynchus*), however, has never been associated with any adverse effect on crop plants, nor habitat destruction; instead, this group of approximately 100 weevil species is known for its striking coloration, which Alfred Russel Wallace described as "surpass(ing) anything found in the whole Eastern hemisphere, if not in the whole world" (see p. 103 of Ref. [17]).

The weevil that is investigated in this work is *Pachyrrhynchus congestus pavonius* (Heller 1921)—an insect found on Luzon, the largest island of the Philippine archipelago. *Pachyrrhynchus congestus pavonius* is shown in Fig. 1. The body and legs are dark and glossy, except for orange annular rings, which are flecked with marginal blue and green scales.

Our interest here is specifically in the orange part of the annular spots. Orange structural coloration is not very common in insects; on the other hand, it is known that the bright coloration of some weevils is caused by the presence of a

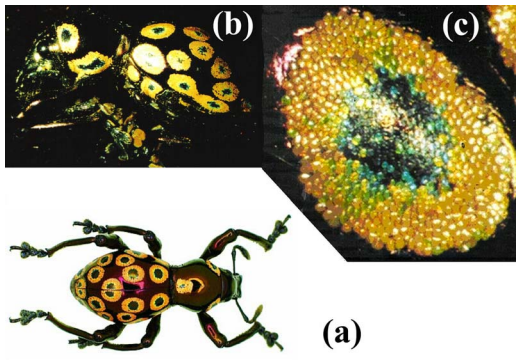

FIG. 1. (Color online) *Pachyrrhynchus congestus pavonius* is a darkly colored weevil, bearing highly conspicuous annular spots on the dorsal and lateral sides of its thorax and abdomen. (a) An entire specimen (not the one used in the study); (b) the specific specimen under investigation; (c) the detail of one spot on the weevil's exoskeleton. The scales are clearly apparent and display a range of colors. The scales of interest are in the orange zones.

*Electronic address: jean-pol.vigneron@fundp.ac.be

three-dimensional structure. This structure can be opal-like (built from tiny chitin spheres [16]); observations of other species suggest an inverse opal, as can be found in Berthier (see p. 158 of Ref. [18]; also see Refs. [19–21]). The objective of this work is to build upon these observations by elucidating the precise geometry of the color-producing structure in the scales of this (previously unexamined) weevil species and relating this geometry to its measured optical properties, using a combination of electron microscopy, optical spectroscopy, and numerical modeling.

II. OBTAINING SAMPLES

Weevil samples were obtained from a commercial insect supplier, who identified them to subspecies level as *Pachyrrhynchus congestus pavonius*. This identification was checked by comparing the insects obtained with museum specimens and with descriptions in the literature [22].

III. REFLECTANCE FROM THE ORANGE SCALES

The normal-incidence specular reflectance from the orange scales was measured with an Avaspec 2048/2 optical-fiber spectrometer. The sample was first placed on the sample holder of an optical microscope and illuminated through the microscope's lenses by the light from a halogen lamp. The reflected light was collected, again through the microscope's optics, by the aperture of a thin optical fiber probe with low acceptance angle, and diverted to the spectrophotometer. In this way, it was possible to conduct measurements on a specific single scale. The reflected light was compared with the light diffused by a white standard, which followed the same path in the optical microscope. The observed spectrum for the average of several scales is shown in Fig. 2(a). Although some variations exist from one scale to another, the dominant wavelength can be located in a region of very desaturated wavelengths, close to 675 nm: this lies in a pink-orange region of the chromaticity diagram. The spectrum is always broad. A very weak blue reflectance is also perceived, but this weak coloration is not associated with any significant visual effect.

Regarding the broadening, it should first be noted that the numerical aperture of the microscope objective (chosen to fit for the examination of a single scale) is rather large (0.85), with the consequence that the illumination takes place within an angle close to $\Delta\theta \simeq 58°$. This is related to the need for light focusing when selecting a small area for analysis. We see that, when there is a rather large illuminating solid angle, the incidence and emergence angles are loosely defined, and this may impact upon the reflectance spectral resolution. In particular, this arises when the coloring structure uses multilayer interference as part of the physical light filtering mechanism, when the dominant reflected wavelength is allowed to change with the angle of incidence. As an example (which will be useful later), if the spectral sensitivity is

$$\frac{\Delta\lambda}{\Delta\theta} \approx 2 \text{ nm/deg}, \tag{1}$$

we can expect, in the present configuration, a spectral broadening close to $\Delta\lambda = 120$ nm.

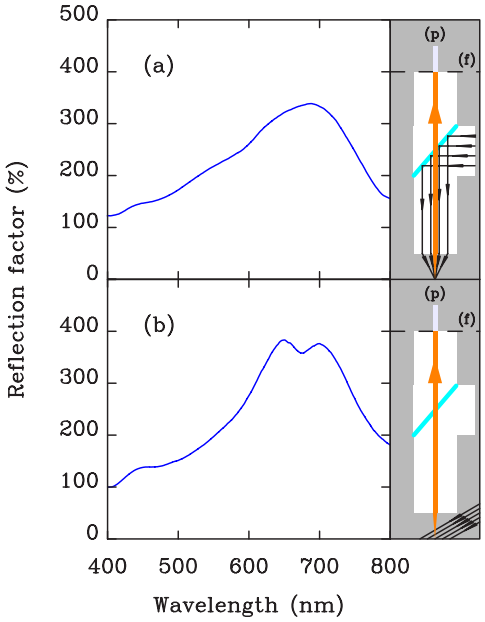

FIG. 2. (Color online) Reflectance spectrum of some orange scales of the weevil *Pachyrrhynchus congestus pavonius*. The dominant wavelength can be located just below 700 nm, but the reflection spectrum is rather broad, extending far into the red and yellow chromatic regions. The spectrum in (a) has been obtained by illuminating and collecting the reflected light through the objective of a microscope. In this case, the incidence angle θ is not well defined, the uncertainty being estimated to reach 58°. This curve is a smoothed average of several orange scales. (b) is the spectrum obtained by illuminating the sample obliquely with a high-intensity parallel beam and collecting the reflected light through the objective of a microscope. In this case, the incidence angle θ is well defined, but cannot be set to zero, because of the volume occupied by the distinct source and collection probes (here, at best, $\theta = 27°$). (p) indicates the thin optical-fiber probe with a low acceptance angle (numerical aperture 0.22) and (f) is the microscope image plane.

Part of this broadening can be eliminated by changing the illumination geometry, at the expense of not being able to carry out a true normal-incidence measurement. Figure 2(b) shows the reflection factor resulting from the use of a nearly parallel beam generated by a high-intensity halogen optic-fiber illuminator, at an incidence of $\theta = 27°$ (the smallest incidence compatible with the shape and volume of the illuminating and collecting probes). As before, the light was collected by the microscope, forming a real image of a single illuminated scale. The fiber-optic probe collects the light only from a specific area (well under the size of the scale image) of this real image. The finite acceptance angle (numerical aperture 0.22) of the fiber-optic probe also severely limits the useful emergence angles (providing some collimation on the reflected beam), so that the attempted interposition of a screen with a pinhole in front of the objective did not improve the resolution. It is clear from Fig. 2(b) that some bandwidth reduction is gained with this geometry, but also that the overall response function of the scale remains broad, and still produces a desaturated pink-orange color.

Unexpectedly, the orange color displayed on the weevil's rings is quite stable when the viewing angle is changed. This

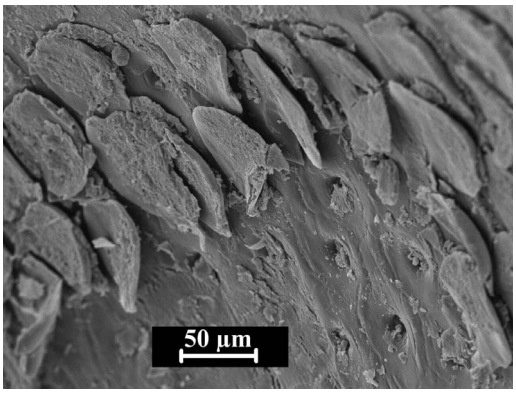

FIG. 3. Scanning electron microscope image of the weevil dorsal area, showing the scales and the scars left on the cuticle when the scales are removed.

is perceptible on images like those in Fig. 1(a) or Fig. 1(b), where, under a well-defined incidence, the colored rings are visible, with the same color, in spite of the fact that the normal to the cuticle surface, at the ring center, varies considerably from one ring to another. This suggests that the optical device that produces the coloration is not exactly an ideal photonic crystal (such a structure would produce very sharp reflection bands that change in dominant wavelength with the angle of incidence—see, for instance, Ref. [13] or [23]). The optical properties shown here are, to some extent, better described as diffuse scattering than reflection or Bragg diffraction, although, as will be shown below, they are explained by a photonic-crystal reflectance effect. The interpretation of these optical properties should take account of the ultrastructure of the scales, as revealed by electron microscopy investigations in the next section, but also consider the lack of iridescence (the change of color with viewing angle).

IV. SCANNING ELECTRON MICROSCOPY

The weevil cuticle is smooth on a large part of the body (the dark sepia and black areas), but, as seen in Fig. 3, the orange regions are covered with discerniable scales. These scales are each attached to the exocuticle through a single pedicle and can be easily removed individually. The small scar remaining after the removal of a scale can also be seen in Fig. 3. The scale length is of the order of 100 μm, the width 50 μm, and the thickness 5 μm.

Each scale is structured as shown in Fig. 4. The straight section normal to the scale's long axis shows a layered external "cortex" or "envelope" of chitin, which protects a very regular three-dimensional structure. The outermost side of this layered cortex (relative to the weevil) is somewhat less than 2 μm thick, while the innermost portion of the cortex (that between the weevil's body and the scale) is much thinner. The volume of the scale is filled with an extremely well-ordered material, which can be viewed as a set of strongly corrugated sheets, parallel to the scale surface. This rigid structure is a three-dimensionally periodic structure, with two optical media: chitin and air. A typical length scale of about 300 nm describes the spatial organization of the structure and suggests its importance for the spectral filtering of visible light.

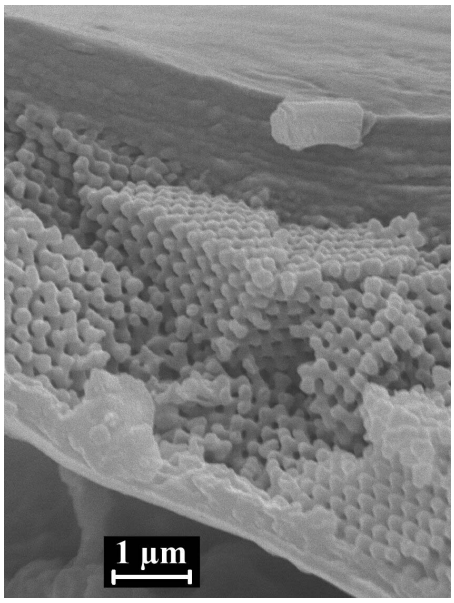

FIG. 4. Section of a scale normal to its surface and to its longitudinal axis. This scanning electron microscope SEM view shows the internal structure of the scales. The layered structure is apparent, but very regular fractures in the direction roughly normal to the layers indicate a highly correlated stacking of these layers.

The apparent periodic geometry shows that the material filling the scale volume is a photonic crystal. The air-chitin refractive index contrast is, of course, too small to generate omnidirectional band gaps, but, in order to explain the reflectance, the important issue is to determine whether stop bands can be found in the visible range, contributing to a spectrally selective diffusion. The photonic crystal, as observed, is not perfect: slight variation in the diameter of the perforations occurs within a sheet and the orientation of the lattice is not constant. Indeed, as seen in Fig. 5, domains with distinct orientations can be identified and this adds to the complexity of the photonic response. The modeling of such a structure calls for two distinct steps: first, the identification of the reflectance of an ideal photonic-crystal structure with parameters extracted from the SEM pictures, and, second, consideration of the effect wrought by the polycrystalline superstructure and the loss of long-range coherence on the optical properties.

V. LOCAL PHOTONIC CRYSTAL

A. Geometric parameters

The electron microscope images (see Figs. 4 and 5) show a stack of perforated plates, which are arranged on top of each other in a geometrically coherent way. Though scanning electron images each convey limited information, due to the two-dimensional presentation of the data, it is possible to assess the present structure rather accurately. The visible part of the structure, in Fig. 5, is the topmost layer, which appears as a thin plate of chitin, perforated by a series of circular

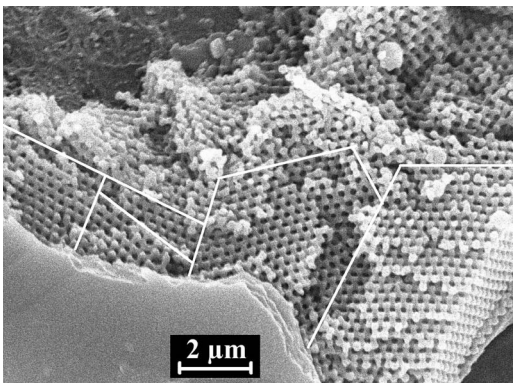

FIG. 5. Scanning electron microscope image of the internal structure of a scale, showing the layered organization. The layers appear to be made from a chitin sheet, perforated by a triangular lattice, with a unit cell containing one hole and one protrusion. Some long-range spatial incoherence is also observed, suggesting a superstructure with domains showing a variable orientation. This kind of structure is better described as a photonic polycrystal than as a photonic crystal.

holes, arranged along a two-dimensional triangular lattice. This single-layer structure is idealized on Fig. 6, which shows the chitin plates and a periodic array of cylindrical holes and protrusions. The distance between the centers of any two neighboring holes is $d=333\pm3$ nm, a value that can be rather precisely known from the electron microscope images, because of the mid-range coherence, and assuming a perfect hexagonal symmetry, which allows us to estimate the surface normal deviation from the view axis, on the two-dimensional image. The radius of the holes can also be estimated to $h=76$ nm from the images, although with less accuracy (±8 nm). Protrusions show the same diameter $b=76$ nm.

The analysis of the possible stacking schemes which respect the structure symmetry (reported in Appendix B at the end of the paper) shows that the corrugated plates are stacked in such a way that the resulting structure has a cubic symmetry. To this end, the protruding (A), flat (B), and empty (C) sites (see Fig. 7) must be aligned vertically, and repeated in that order (ABC stacking). The stacking distance between

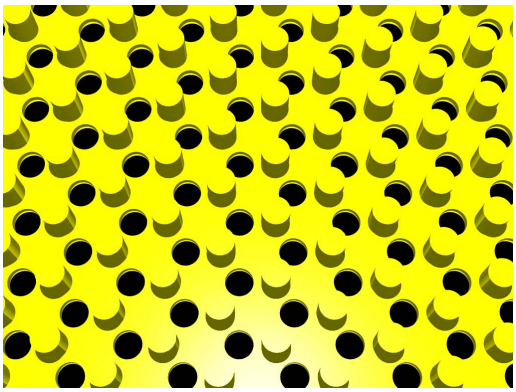

FIG. 6. (Color online) Idealized structure of a chitin layer, which incorporates the geometry parameters deduced from an analysis of the SEM images.

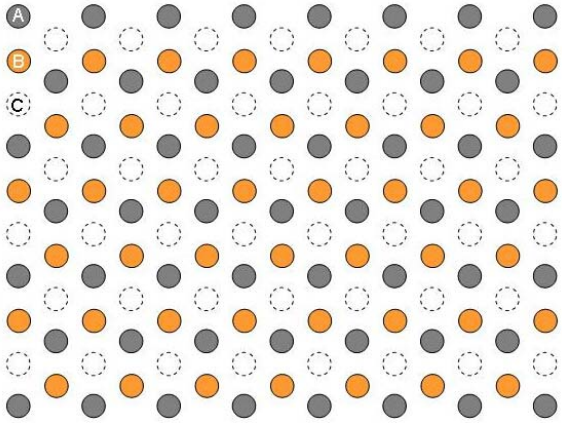

FIG. 7. (Color online) The basic layer of the weevil scale structure is invariant under the translations of a triangular lattice. In the primitive cell, we find the elements for three coexisting sublattices: a sublattice of protrusions acting as spacers (A sites), a sublattice of empty sites (B sites), and a sublattice of holes (C sites).

A and B layers, and between B and C layers must be $p=272$ nm for a cubic structure, and this can be verified on some scanning electron images, confirming the structure symmetry. The protrusion height can be estimated by inspection of the scanning electron microscope images, and a value of 214 nm can be retained, leaving an average chitin plate thickness of 58 nm.

With these numbers, it is relatively easy to determine the filling factor f of the crystal structure, i.e., the ratio between the volume occupied by chitin and the total cell volume. The volume of the primitive cell, containing one hole and one protrusion, is easily evaluated to 78.3×10^6 nm^3, while the sum of the volumes of the three equivalent chitin sheets (bearing the protrusions) in the primitive cell, reduced by the volume of the hole, gives a chitin volume per cell of 25.2×10^6 nm^3. This leads to a filling factor $f=0.32$. Using an approximate value $n=1.56$ for the chitin refractive index (see, for instance, Ref. [24]), the average value of the dielectric constant can then be estimated as

$$\langle\varepsilon\rangle = f(1.56)^2 + (1-f)(1)^2 = 1.46 \tag{2}$$

(which corresponds to a refractive index of 1.2) or

$$\left\langle\frac{1}{\varepsilon}\right\rangle = f\frac{1}{(1.56)^2} + (1-f)\frac{1}{(1)^2} = \frac{1}{1.23} \tag{3}$$

(which means a refractive index of 1.1), depending on the orientation of the surfaces with respect to the radiation's electric field. Actually, both averaging formulas lead to roughly similar results, and the following estimation of the average refractive index for the whole photonic crystal should be reliable enough for our present purpose:

$$\bar{n} = \sqrt{\frac{1.46+1.23}{2}} = 1.16. \tag{4}$$

B. Dominant reflected wavelength

Before embarking on detailed numerical simulations of the reflectance of the layer structure described above, we can, at least for the case of near-normal incidence, determine the dominant reflected wavelength from such a photonic crystal. We relate the reflection to the presence of photonic-crystal stop bands and we estimate the spectral location of these bands by assuming an infinite repetition of the three-layer period shown in Fig. 7. We also assume weak refractive index differences and we average the structure in planes parallel to the layers: this procedure, in principle, is valid only for incident waves sent close to normal incidence, when the wave periodicity parallel to the interfaces becomes much larger than the typical corrugation length in these directions. With all of these assumptions, reflection occurs at angular frequencies ω where a photonic gap occurs, i.e., when the average dispersion relation

$$\omega = k\frac{c}{\bar{n}} \tag{5}$$

crosses a Brillouin zone boundary (k is the norm of the wave vector in the averaged medium, and c is the light propagation speed in vacuum). This occurs at wavelengths λ such that

$$\lambda = \frac{2p\bar{n}}{m}, \tag{6}$$

where p is the multilayer periodicity (here, one-third of the real three-dimensional ABC periodicity, as the shifted layers are "smeared," and made equivalent, by lateral averaging), and m is an integer that brings the frequency into the range of interest (i.e., here, the visible spectral range). In a straightforward way, we obtain (with, as mentioned above, a period $p=272$ nm)

$$\lambda = \frac{2 \times 272 \times 1.16}{1} = 631 \text{ nm}. \tag{7}$$

This wavelength is clearly in the orange-red part of the visible spectrum and compares reasonably (for a broad band such as that observed here) with the dominant color revealed by the measured spectra in Fig. 2. The structure just described, then, explains the dominance of an orange reflection from the scales in the annular markings of the weevil.

C. Ideal photonic-crystal reflectance spectrum

We can proceed with a more complete investigation of the reflectance spectrum. The reflectance can be calculated from the geometry described in Sec. V A if we completely ignore the superstructure of misoriented domains observed in Fig. 5 and idealize the structure to fit a perfect photonic-crystal film (composed of a dozen layers). This computation uses a three-dimensional transfer-matrix technique [23,25] and includes multiple-scattering effects at all orders. It is suitable for providing simulations of the specular and diffracted reflections as a function of the incident wavelength, the incidence angle, the azimuthal incidence angle, and the incident-wave polarization state. In Fig. 8, the reflectance spectrum is calculated for a stack of 16 three-layer periods, assuming a strict normal incidence, and using the geometric and optical parameters described above. The number of field harmonics used in the calculation was limited to 64, and only the transverse-electric incidence light was considered (transverse-magnetic light gives similar results). The calculated reflectance spectrum under normal incidence turns out to be very simple: it displays a sharp reflection band centered near 650 nm, in the red-orange spectral region. This is in good agreement with the dominant wavelength estimated in Sec. V B and with the broad experimental spectrum (see Fig. 2). The calculated line shape, however, does not fit the measured spectrum. More puzzling is the fact that the spectral location of the reflected band changes with the incidence angle: an iridescence effect which is observed neither with the spectrophotometer nor by the naked eye.

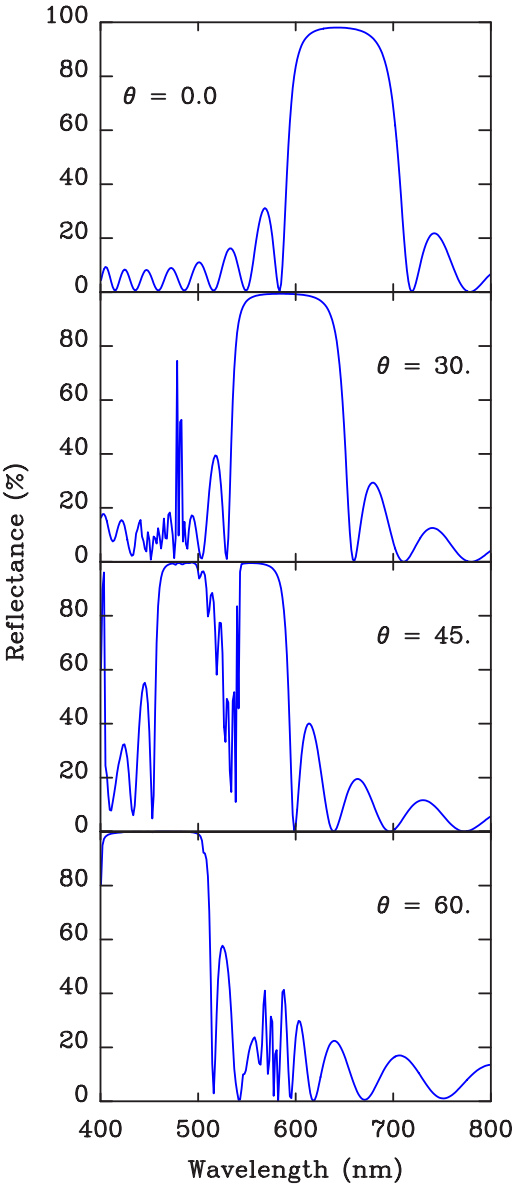

FIG. 8. (Color online) Calculated specular reflectance of a stack of layers shown in Fig. 7, arranged to form a face-centered cubic lattice, for four angles of incidence $\theta=0°$ (normal incidence) to 60°. Note the shift of the spectrum as the incidence angle is increased.

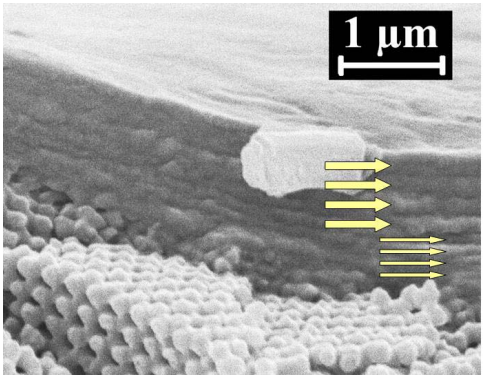

FIG. 9. (Color online) Detail of the layered cortex, which constitutes the outer part of a scale. This structure actually contains two distinct selective mirrors: the upper one reflects yellowish green light (peak wavelength 528 nm), while the one just below reflects purplish blue (peak wavelength 447 nm).

D. Polycrystal chaotic reflectance

The above results from a perfect photonic crystal show that, while an ideal structure can account crudely for the orange coloration of the weevil's scales, it cannot explain the broad spectrum observed experimentally. Figures 2(a) and 2(b) show that, in the measurement, the numerical aperture tends to broaden the spectrum, but when every effort is made to improve this, spectral features, such as the line shape, remain that still need to be explained.

The scale of the weevil is not an infinite semicrystal, as first assumed above. The material inside the scale shows domains and irregular interfaces between domains, which cause light diffusion. With multiple scattering, such diffused waves meet the reticular planes of the domain crystallites with many different incidence angles, so that the internal incidence angles on the domain's surfaces do not retain any memory of the external incidence angle [26]. This loss of orientational information is a chaotic behavior, which can occur with even a very small number of crystallite interfaces inside the scale cavity. It essentially has two consequences. The first is to decorrelate the emergent and the incident wave directions, so that the illuminated surface loses much of the metallic appearance expected for a short-period three-dimensional photonic crystal and the color seen under most viewing angle is averaged and angularly stabilized, avoiding iridescence. The second one is that the spectrum will be smeared out, because for any external incidence we will be able to find a range of internal incidences in the multiply scattered beam and, from these, a wider range of wavelengths will be selected.

We investigated this chaotic behavior by computing numerically a spectrum that contains, in a uniform way, all incidences (zenithal and azimuthal) on the surface of the photonic crystal with the structure described in Sec. V A. Taking all possible orientations is most certainly a simplification, but our SEM observations did not clearly suggest any orientational constraints. Furthermore, the incident beam entering the scale is not only randomly redirected by the grain boundaries: it is also redistributed by reflections, from inside, taking place on the scale cortex. Because of this, even in the situation of a constrained orientational disorder (as, for instance, in a two-dimensional "mosaic" grain arrangement) the beam orientation distribution will be three dimensional. The result of this orientational averaging is shown in Fig. 10, which should be compared to the reflection factor measured and represented in Fig. 2. One immediately sees that, even if the calculation locates the reflection band at wavelengths slightly shorter than observed, the agreement is reasonable for both the dominant wavelength (and hence the predicted color) and the bandwidth (and hence the desaturation) and considerably improves the line shape. As in the experimental spectrum, the reflectance exhibits a double peak with distinctive components separated by about 50 nm.

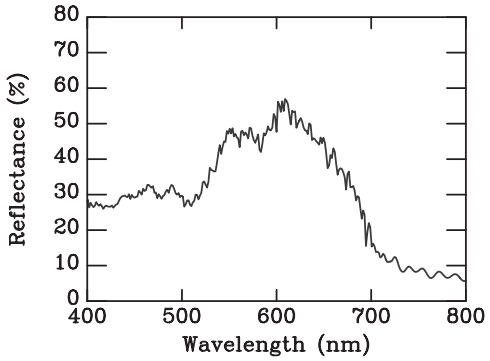

FIG. 10. Hemispherical reflectance of the ideal weevil scale photonic crystal, averaged over the incidences in the entire illumination hemisphere (zenithal and azimuthal angles). The experimental reflection factor reported on Fig. 2 is modeled better by such an average, because of the chaotic scattering induced by the polycrystalline nature of the photonic structure which produces a filtered reflection. This transfer-matrix calculation converged with only 16 Fourier components.

This chaotic reflection, due to the presence of domains in the photonic material of the scales, means that the emerging light has lost the memory of the external incidence direction. The consequence is that, whatever the illumination setup, the same orange coloration of the rings will be seen from everywhere. It also means that the color filtering will not depend strongly on the illumination and viewing directions, although the building block of the polycrystal photonic structure would, alone, produce a strong iridescence.

Breaking iridescence with a polycrystal is not a completely new mechanism in nature. The Brazilian butterfly *Cyanophrys remus*, for instance (and probably many others that have not been fully investigated), has been shown to use a photonic polycrystal on the ventral scales to produce a noniridescent pea-green cryptic coloration [27].

E. Side contributions

The face-centered cubic material only fills the interior of the scale: the external part is a cortex, which is more than 1 μm thick, and, as can be seen in Fig. 9, is actually formed by two types of layers. The four exterior most layers, just below the surface of the scale, have each a thickness of 176 nm. As the average refractive index of the cortex must

be close to $\bar{n}=1.5$ (a little less than the index of pure chitin), the dominant reflection wavelength must be

$$\lambda = 2 \times 176 \times 1.5 = 528 \text{ nm}. \quad (8)$$

This is not visible in the experimental reflection, possibly because of the very small number of interfering waves in this very thin structure. It is interesting to note that the small bump just below 450 nm in the experimental reflectance could also be tentatively explained by the structure of the cortex. The deeper layers, in contact with the inverse-opal-like filling, have a thickness of 149 nm, from SEM observation. The reflection wavelength associated with these layers can be calculated as before:

$$\lambda = 2 \times 149 \times 1.5 = 447 \text{ nm}, \quad (9)$$

and this coincides with the purplish-blue bump. If this is true, we have, in *Pachyrrhynchus congestus pavonius*, a three-component dielectric mirror, but in contrast to other broadband mirrors, which make use of stacked one-dimensional multilayers [28], the present one combines two multilayers and a special, three-dimensional polycrystal. This very evolved structure is probably worth further study, and the investigations should probably not be limited to the mechanisms of optical reflection.

VI. CONCLUSION

In this work, we have shown that the orange coloration of the weevil *Pachyrrhynchus congestus pavonius* is associated with the three-dimensional structure that fills the scales of the colored rings. The crystal structure has been identified as a photonic polycrystal, the crystallites (or domains) being organized as a face-centered cubic crystal; this structure develops as a stack of layers invariant under the translations of a triangular lattice. A two-stage model was developed, which idealizes the observed geometry. This model complies with the data that was obtained from the SEM images and assumes a cubic symmetry. The first stage of the model idealizes the structure as a coherent photonic-crystal film that is infinite in the lateral directions. This leads to reflection bands, which shift to shorter wavelengths with increasing incidence angles. If the order of magnitude of the reflection wavelengths is acceptable, the line shape of the reflection bands near normal incidence and the predicted iridescence contradict observations, both experimental and with the naked eye. The second stage of the model repairs these paradoxical results, by accounting for internal scattering due to the presence of crystal domains varying in orientation and separated by diffusive interfaces. The presence of these defects leads to isotropic scattering which strongly decorrelates the incident and emergent light beams. This loss of memory of the beam orientation explains both the diffuse scattering produced by the photonic structure and the broad spectrum actually observed.

The coloration of this genus of weevils is among the most astonishing visual effects displayed in nature. Many animal species that are distasteful to predators have evolved aposematism (they have a distinctive, conspicuous coloration, which functions as a warning signal, advertising their inedibility to potential predators). Wallace notes in a passage on the genus *Pachyrrhynchus* (see p. 292 of [29]) that many weevils have excessively hard integuments, which render them inedible to most birds, and our own dissections of this species confirm their extremely tough exoskeleton. It seems likely, therefore, that the stark coloration of this species is a form of aposematism. Further evidence in support of this comes from the finding that a number of edible species, such as the longicorn beetles *Doliops curculionides* and *Doliops geometrica* and the cricket *Scepastus pachyrhynchoides* mimic various *Pachyrrhynchus* species weevils [29].

ACKNOWLEDGMENTS

We wish to thank Darren Mann of Oxford University Museum of Natural History and Max Barclay of the Natural History Museum in London for facilitating access to these museums' collections and to Darren Mann additionally for assistance tracing some of the literature on the genus *Pachyrrhynchus*. This work was carried out with support from EU5 Centre of Excellence Grant No. ICAI-CT-2000-70029 and from the Inter-University Attraction Pole (IUAP P5/1) on "Quantum-Size Effects in Nanostructured Materials" of the Belgian Office for Scientific, Technical, and Cultural Affairs. The authors acknowledge the use of Namur Interuniversity Scientific Computing Facility (Namur-ISCF), a common project between the Belgian National Fund for Scientific Research (FNRS) and the Facultés Universitaires Notre-Dame de la Paix (FUNDP). This work was also partly supported by the European Regional Development Fund (ERDF) and the Walloon Regional Government under the "PREMIO" INTERREG IIIa project. The work was also supported in part by an EU6 BIOPHOT/NEST grant. V.L. was supported by the Belgian National Fund for Scientific Research (FNRS). V.W. was supported for part of this work by the Royal Commission for the Exhibition of 1851 and the Belgian FNRS. The authors thank Professor Amand Lucas for many suggestions.

APPENDIX A: INCIDENCE ANGLE DEFINITION IN MICROREFLECTANCE MEASUREMENTS

As discussed in the text, a microspectrophotometer can be used to measure the reflectance from small areas, which is important here, as the scales of the weevil (about 50 μm in diameter) just occupy thin circular rings on the weevil cuticle. The instrument is basically a microscope that is able to provide illumination focused on the object, through the objective. The scattered light returns to the objective and converges back to form an image, a small portion (pixel) of which is sent to the spectrophotometer. The conditions for the measurement are restrictive. Long-focal objectives define the incidence angle pretty well, but form an image of low magnification, which is not suitable for spectral analysis of a pointlike object. Short-focal objectives provide higher magnifications but the numerical aperture is larger and the incidence angle is less well defined. When the reflectance bands shift with varying incidences, the uncertainty of the incidence angle can limit the spectral resolution of the measure-

ment. Restriction of the acceptance angle of the objective by a diaphragm can improve the situation, but reduces the intensity of the light being measured.

In the present work, the measurement was improved by first using an external illuminator (150 W) providing a nearly parallel incident beam (10° divergence) and collecting the light through a diaphragm and the objective of a microscope, collecting the light by an optic-fiber probe in the image plane of the microscope. In this arrangement, the optic fibre, which has a numerical aperture 0.22, provides a collimating effect, so that the measurement is not drastically altered by closing the diaphragm.

APPENDIX B: SYMMETRY OF THE THREE-DIMENSIONAL PHOTONIC-CRYSTAL STRUCTURE IN THE WEEVIL'S SCALE

In this appendix, we give more details on the analysis of the SEM images, leading to the conclusion that the layered slabs of triangular symmetry can be stacked to form a photonic crystal structure with a face-centered cubic lattice.

On the perforated and bumpy slabs revealed by SEM (see Sec. IV), each hole has six nearest neighbors and lies at the center of a regular hexagon formed by these neighbors. The distance between the centers of any two neighboring holes is, as mentioned above, $d=333$ nm, from center to center. The triangular lattice of holes leaves two other, inequivalent, sites with the full triangular symmetry. One of them is occupied by a protrusion with a shape between hemispherical and cylindrical. It is somewhat more difficult to assess the diameter of the protrusions, but since the distance between neighboring triangular site in this crystal structure is $d/\sqrt{3}$, the space left for the protrusion base limits its radius to $b<116$ nm. Inspection of the SEM images indicates that, in fact, the protrusion diameter is of the same order as the diameter of the holes, so that we can model the structure with $b=h=76$ nm. On the SEM views, these protruding spacers are apparent in Fig. 5, from an appropriate perspective, and less visible under a strict normal observation. The cylindrical spacers are distributed on a triangular lattice similar to the lattice of holes, except for a constant translation of length $d/\sqrt{3}$. This translation brings them to equal distances from their three neighboring holes. The third triangular site, not occupied by a hole or a protrusion, is empty and simply offers a view of the chitin sheet.

The corrugated and perforated slabs are stacked on top of each other in a direction normal to the surface of the scale, in such a way that each perforated slab runs parallel to the surface of the scale. The stacking of such a hexagonal structure, while keeping all C_{3v}-symmetry sites (those sites where 120° vertical-axis rotations leave the structure invariant), can be obtained in just three different ways and the examination of the SEM pictures helps us to choose the correct one. In the following discussion, we will name the three C_{3v}-symmetry sites in the following way (see Fig. 6): the *A* site is the protrusion-center location, the *B* site is the empty C_{3v} site, and the *C* site is the hole-center location. The stacking options are then not so numerous. On top of the protrusion, we can have either an *A* site, a *B* site, or a *C* site. Starting with the *A* site and then again would mean an *AAA*… stacking, where the holes would form a rectilinear free channel, which is not observed. The *ACAC*… stacking would force the matching of a protrusion with a hole, which is mechanically awkward and is not observed either. The *AB* stacking assumes contact of the protrusion with the chitin plate at the empty site, and implies another move of the third layer, which brings the *C* site over the empty *B* site. The stacking is then actually of the type *ABCABC*…. The shift of each successive layer is 192 nm in this model, in good agreement with the observations. This oblique alignment of the layers can be seen, for instance, in SEM pictures such as Fig. 4. We note that the *AAA*… stacking would give rise to the simple hexagonal lattice, the *ABAB*… stacking would lead to the hexagonal compact lattice, while the *ABCABC*… stacking leads to the face-centered cubic lattice, if the distance between the layers matches the appropriate symmetry requirement. Fractures containing the normal to the layers exist on the prepared samples, and on these faces a hexagonal structure also reveals itself. Furthermore, no compression of the hexagonal cells is perceived, so that the exact face-centered cubic structure can be assumed. In such a structure, the distance between *A* and *B* layers and the distance between *B* and *C* layers are given by $p=a/\sqrt{3}$, where $a=d\sqrt{2}=471$ nm, which means $p=272$ nm.

The protrusion height can be estimated from inspection of the SEM images, and a value of 214 nm can be obtained. This leaves a chitin plate thickness of 58 nm. This is a rather thin plate, but this simply means that the roughly cylindrical "spacers" play an important role in explaining the reflectance. In three dimensions, these scatterers are distributed on a face-centered cubic lattice. The structure can then be called an opal or an inverse opal (even if we recognize that the structure is not exactly an assembly of spheres), according to the filling factor of the structure (the ratio of the chitin volume per cell to the complete cell volume). More chitin than air defines the opal, while more air than chitin should rather define the inverse opal.

[1] J. Zi, X. Yu, Y. Li, X. Hu, C. Xu, X. Wang, X. Liu, and R. Fu, Proc. Natl. Acad. Sci. U.S.A. **100**, 12576 (2003).

[2] J. P. Vigneron, J.-F. Colomer, M. Rassart, A. L. Ingram, and V. Lousse, Phys. Rev. E **73**, 021914 (2006a).

[3] A. R. Parker, R. C. McPhedran, D. R. McKenzie, L. C. Botten, and N. A. Nicorovici, Nature (London) **409**, 36 (2001).

[4] V. Welch, J. P. Vigneron, V. Lousse, and A. Parker, Phys. Rev. E **73**, 041916 (2006).

[5] H. Ghiradella, D. Aneshansley, T. Eisner, R. E. Silberglied, and H. E. Hinton, Science **178**, 1214 (1972).

[6] H. Tada, S. E. Mann, I. N. Miaoulis, and P. Y. Wong, Appl. Opt. **37**, 1579 (1998).
[7] S. Yoshioka and S. Kinoshita, Proc. R. Soc. London, Ser. B **271**, 581 (2004).
[8] C. R. Lawrence, P. Vukusic, and R. Sambles, Appl. Opt. **41**, 437 (2002).
[9] P. Vukusic, J. R. Sambles, C. R. Lawrence, and R. J. Wootton, Nature (London) **410**, 36 (2002).
[10] A. Argyros, S. Manos, M. C. J. Large, D. R. McKenzie, G. C. Cox, and D. M. Dwarte, Micron **33**, 483 (2002).
[11] Z. Vertezy, Z. Balint, K. Kertesz, D. Mehn, I. Kiricsi, V. Lousse, J.-P. Vigneron, and L. Biro, Microscopy and Analysis **18**, 25 (2004).
[12] D. G. Stavenga, S. Stowe, K. Siebke, J. Zeil, and K. Arikawa, Proc. R. Soc. London, Ser. B **271**, 1577 (2004).
[13] J. P. Vigneron, M. Rassart, C. Vandenbem, V. Lousse, O. Deparis, L. P. Biró, D. Dedouaire, A. Cornet, and P. Defrance, Phys. Rev. E **73**, 041905 (2006).
[14] A. C. Neville and S. Caveney, Biol. Rev. Cambridge Philos. Soc. **44**, 531 (1969).
[15] J. P. Vigneron, J.-F. Colomer, N. Vigneron, and V. Lousse, Phys. Rev. E **72**, 061904 (2005).
[16] A. R. Parker, V. L. Welch, D. Driver, and N. Martini, Nature (London) **426**, 786 (2003).
[17] A. R. Wallace, Br. Assoc. Adv. Sci., Rep. **46**, 100 (1876).
[18] S. Berthier, *Iridescences, les Couleurs Physiques des Insectes* (Springer-Verlag, Paris, 2003).
[19] H. Ghiradella, Ann. Entomol. Soc. Am. **77**, 637 (1984).
[20] V. L. Welch, in *Structural Colours in Biological Systems—Principles and Applications*, edited by S. Kinoshita and S. Yoshioka (Osaka University Press, Osaka, 2005).
[21] A. Parker, SPIE Newsroom doi:10.1117/2.1200604.0237 (2006).
[22] W. Schultze, Philip. J. Sci. **24**, 309 (1924).
[23] J. Vigneron and V. Lousse, Proc. SPIE **6128**, 61281G (2006).
[24] B. Gralak, G. Tayeb, and S. Enoch, Opt. Express **9**, 567 (2001).
[25] J. B. Pendry and A. MacKinnon, Phys. Rev. Lett. **69**, 2772 (1992).
[26] J. Schroeder and J. H. Rosolowski, Proc. SPIE **297**, 156 (1981).
[27] K. Kertész, Z. Bálint, Z. Vértesy, G. I. Márk, V. Lousse, J. P. Vigneron, M. Rassart, and L. P. Biró, Phys. Rev. E **74**, 021922 (2006).
[28] A. R. Parker, D. R. M. Kenzie, and M. C. J. Large, J. Exp. Biol. **201**, 1307 (1998).
[29] A. R. Wallace, in *Science for All*, edited by R. Brown (Cassell, Petter, Galpin and Co., London, 1879), Vol. 2.